Cement and Concrete Research 41 (2011) 218–229

Contents lists available at ScienceDirect

Cement and Concrete Research

journal homepage: http://ees.elsevier.com/CEMCON/default.asp

The origin of early age expansions induced in cementitious materials containing shrinkage reducing admixtures

Gaurav Sant [a,*], Barbara Lothenbach [b,1], Patrick Juilland [c], Gwenn Le Saout [b,2], Jason Weiss [d,2], Karen Scrivener [e,3]

[a] Department of Civil and Environmental Engineering, 420 Westwood Plaza, 5731 Boelter Hall, University of California, Los Angeles, CA 90095-1593, United States
[b] EMPA, Swiss Federal Laboratories for Materials Testing and Research, Laboratory for Concrete and Construction Chemistry, Überlandstrasse 129, CH-8600 Dübendorf, Switzerland
[c] Ecole Polytechnique Fédérale de Lausanne, Laboratory of Construction Materials, Ecublens, CH-1015, Lausanne, Switzerland
[d] Purdue University, School of Civil Engineering, 550 Stadium Mall Drive, West Lafayette, IN, USA
[e] Ecole Polytechnique Fédérale de Lausanne, Station 12, MXG-211, Ecublens, CH-1015, Switzerland

ARTICLE INFO

Article history:
Received 17 March 2010
Accepted 16 December 2010

Keywords:
Expansion [C]
Pore solution [B]
Shrinkage [C]
Shrinkage reducing admixture
X-ray diffraction [B]

ABSTRACT

Studies on the early-age shrinkage behavior of cement pastes, mortars, and concretes containing shrinkage reducing admixtures (SRAs) have indicated these mixtures frequently exhibit an expansion shortly after setting. While the magnitude of the expansion has been noted to be a function of the chemistry of the cement and the admixture dosage; the cause of the expansion is not clearly understood. This investigation uses measurements of autogenous deformation, X-ray diffraction, pore solution analysis, thermogravimetry, and scanning electron microscopy to study the early-age properties and describe the mechanism of the expansion in OPC pastes made with and without SRA. The composition of the pore solution indicates that the presence of the SRA increases the portlandite oversaturation level in solution which can result in higher crystallization stresses which could lead to an expansion. This observation is supported by deformation calculations for the systems examined.

1. Introduction and background

Since their introduction approximately three decades ago, shrinkage reducing admixtures (SRAs) have been extensively advocated as a methodology for reducing shrinkage and cracking in cement-based materials [1–8].

While the majority of studies performed have reported reductions in drying shrinkage [1–3,6], other studies have evaluated the influence of SRAs on evaporation, plastic shrinkage, autogenous deformation and self-desiccation at early-ages [9–15]. Under drying conditions, the SRA is observed to increase the volume of pores that empty at a given relative humidity thus altering the humidity range over which capillary stresses dictate the shrinkage response [10,15]. On the other hand, under autogenous conditions, the reduction in the surface tension of the pore solution by the SRA reduces the development of capillary stresses and maintains a higher internal relative humidity in sealed systems resulting in a reduction in shrinkage [10,11,13,16].

Studies of autogenous deformations on cementitious materials indicate that the addition of an SRA can result in a period of expansion which in turn induces a compressive stress in the system [10,17]. This period of expansion, which initiates shortly after set provides a considerable benefit in shrinkage mitigation even at longer time scales [10,18]. The impact of the expansion in mitigating autogenous shrinkage is considerable, as the expansion can amount to up to 60% of the reduction in unrestrained shrinkage under sealed conditions [10,11]. This indicates that a large part of the reduction in autogenous shrinkage by SRAs arises from the expansion.

This study takes a multidisciplinary approach to examine hypotheses associated with the nature of the expansion observed in mixtures containing SRAs. The results have important implications in understanding the reduction in shrinkage and stress development and the risk of cracking observed in concretes containing SRAs and developing material property inputs for simulation models which aim to predict the risk of cracking in restrained concrete elements.

2. Materials, mixture compositions and mixing procedures

A Type I, ASTM C150 compliant, portland cement with a Blaine fineness of 360 m^2/kg was used in this study. The composition of the cement as determined using quantitative X-ray diffraction indicated a phase composition (mass-basis) of 59.2% $3CaO{\bullet}SiO_2$, 15.5% $2CaO{\bullet}SiO_2$,

* Corresponding author. Tel.: +1 310 206 0497; fax: +1 310 206 2222.
E-mail addresses: gsant@ucla.edu (G. Sant), barbara.lothenbach@empa.ch (B. Lothenbach), patrick.juilland@epfl.ch (P. Juilland), gwenn.lesaout@empa.ch (G. Le Saout), wjweiss@purdue.edu (J. Weiss), karen.scrivener@epfl.ch (K. Scrivener).
[1] Tel.: +41 44 823 4788; fax: +41 44 823 4035.
[2] Tel.: +1 765 494 2215; fax: +1 765 494 0395.
[3] Tel.: +41 21 693 2843; fax: +41 21 693 5800.

0008-8846/$ – see front matter © 2010 Elsevier Ltd. All rights reserved.
doi:10.1016/j.cemconres.2010.12.004

Table 1
The proportions of the cement paste mixtures investigated (mass fraction).

Mixture ID	Cement paste mixtures	
	$w/c = 0.30$	$w/c = 0.30$SRA
Cement	1.000	1.000
Water	0.300	0.285
Tetraguard AS20	–	0.015
Glenium 3000NS	0.005	0.005

11.6% $3CaO{\bullet}Al_2O_3$, and 4.3% $4CaO{\bullet}Al_2O_3{\bullet}Fe_2O_3$, 1.4% $CaSO_4{\bullet}2H_2O$, 2.2% $CaSO_4{\bullet}0.5H_2O$, 0.4% $CaSO_4$, 0.5% $Ca(OH)_2$, 2.7% $CaCO_3$, 2.3% K_2SO_4.

Two mixtures (Table 1) were evaluated in this study, a plain cement paste and a cement paste containing a shrinkage reducing admixture. The cement pastes were prepared using a planetary mixer as described in ASTM C305 [19]. To enhance the workability of the mixtures a water-reducing admixture (WRA) Glenium 3000NS was added at the rate of 0.5% by mass of the cement. A shrinkage reducing admixture (SRA, Tetraguard AS20 [20]) was added to the cement paste mixture at a 5% concentration of the initial water-SRA solution (by mass replacement). Unless noted otherwise, the experiments were performed at room temperature, i.e., 20–23 °C.

3. Experimental procedures

3.1. Isothermal conduction calorimetry

A TamAir isothermal calorimeter was used to determine the heat evolved during the hydration reaction under a constant temperature condition (20 °C). The thermal power and energy measured were used to assess the kinetics and the extent of hydration of the cement paste using an ultimate heat release value of 510 J/g for the cement, calculated using its phase composition [21].

3.2. Autogenous deformation – the corrugated tube protocol

Autogenous deformation of the paste mixtures was measured using a technique where the fresh cement paste was encapsulated in corrugated (perpendicular to the long-axis, ASTM C1698) polyethylene molds with a length-to-diameter ratio of 400 mm-to-30 mm [22,23]. Since the corrugated mold has a higher stiffness in the radial direction than in the longitudinal direction, it allows transformation of volumetric deformations into linear deformations while the paste is fluid. The technique is designed to minimize restraint of the fresh paste, thereby permitting measurements to start approximately 30 min after the time of casting. The fresh cement paste was cast into the corrugated tubes and vibrated. The specimen was then placed in a room maintained at 23 ± 1 °C on a dilatometer assembly which was equipped with data-logging and electronic displacement transducers with an accuracy of ± 5 με [23]. The uncertainty of the measurements was determined to be 8%, for measurements zeroed to the time of final set as determined using the Vicat test (ASTM C191); 7 h and 9 h for the plain and SRA systems respectively [12,19].

3.3. Thermogravimetric analysis (TGA/DTG)

Thermogravimetric analysis was carried out on duplicate powdered paste samples after freeze-drying in liquid N_2 to stop hydration at three ages (11, 26, 48 h) using a thermal analyzer manufactured by Mettler Toledo[4] (Model: TGA/SDTA 851e) with a STARe data acquisition interface. The temperature and mass sensitivity of the thermal analyzer used were 0.25 °C and 0.1 μg respectively. The powder samples were heated under N_2 purge at a flow rate of 30 ml/min and at a heating rate of 10 °C/min in pure aluminum oxide crucibles over a temperature range from 30 °C to 1100 °C. The weight loss (TG) and differential weight loss (DTG) patterns acquired were used to identify and quantify the phases present in the system.

3.4. Scanning electron microscopy (SEM)

Scanning electron microscopy was used to examine plane polished sections in backscattered electron mode (BSE) using a FEI Quanta 200 scanning electron microscope equipped with a PGT X-ray analyzer and Spirit Technologies interface for image acquisition. Triplicate paste specimens ($w/c = 0.30$, $w/c = 0.30$SRA) were prepared at two ages (11 and 26 h) after freeze-drying in liquid N_2 to stop hydration. After this time, the specimens were vacuum impregnated with a low viscosity epoxy resin (Epotek 301), polished with diamond grits and carbon-sputter coated prior to microscopic examination. BSE imaging was combined with EDS (energy dispersive X-ray spectroscopy) to identify phases present in the system [24].

3.5. Quantitative X-Ray diffraction using Rietveld refinement (XRD)

X-ray diffraction (XRD) measurements were carried out with a PANalytical X'Pert Pro MPD diffractometer in a θ–θ configuration using Cu-Kα radiation ($\lambda = 1.54$ Å). The samples were scanned between 7 and 70° (2θ) in continuous mode with an integrated step scan of 0.017° (2θ) using a X'Celerator detector. The total time required for acquisition of the X-ray diffraction pattern was 30 min. A fixed divergence slit of 0.5° was used during acquisition. For the X-ray diffraction measurements, approximately 20 cm^3 of cement paste were cast inside plastic vials and sealed immediately after casting. At the desired age, the specimens were demolded, sliced using a water-cooled diamond saw and immediately placed in a circular sample holder for acquisition of an X-ray diffraction pattern. It has been established that this method (without any drying) allows for good quantification of the phase contents in the system [25].

The Rietveld analysis was carried out using the X'Pert HighScorePlus© software using the following structures for the dominant phases in the anhydrous sample and the hydrated paste; monoclinic C_3S, C_2S, C_4AF, cubic C_3A, gypsum, hemihydrate, anhydrite, periclase, portlandite and ettringite [26–34]. In the refinement strategy, while the profile parameters varied (scale factor, the W coefficient to describe the Full-Width at Half-Maximum of the pseudo-Voigt profile function and the lattice parameters), the atomic parameters retained their original values [25]. Preferred orientation corrections for the C_3S, sulfate phases, portlandite and ettringite were made using the March model [35]. The background signal was refined using a high-order polynomial function for the anhydrous cement. In the case of the hydrated cement, if the polynomial function was unable to describe (fit) the amorphous background, a correction using the Sonneveld algorithm was applied before the Rietveld refinement [36,37].

3.6. Pore solution expression and chemical composition analysis

Pore solution was extracted from cylindrical paste specimens ($w/c = 0.30$, $w/c = 0.30$SRA) using nitrogen pressure filtration or a high pressure steel die. Nitrogen pressure filtration was used for specimens in the plastic phase according to the procedure described by Penko [38]. For hardened specimens, a high pressure die with a capacity of 550 MPa was used according to the procedure described by Barneyback and Diamond [39,40]. After extraction, the pore solution was stored in small (2.5 ml) plastic containers and sealed immediately to minimize the potential for carbonation. The ionic composition of the pore solutions

[4] Commercial equipment, instruments, and materials mentioned in this report are identified to foster understanding. Such identification does not imply recommendation or endorsement by the University of California, Los Angeles, Purdue University, the Ecole Polytechnique Fédérale de Lausanne (EPFL) or the Swiss Federal Laboratories for Materials Testing and Research (EMPA) nor does it imply that the materials or the equipment identified are necessarily the best available for the purpose.

was measured at various ages over the first 48 h using a Varian SpectrAA-20 spectrometer for cation analysis, a Dionex BIOLC ion chromatograph for sulfate ion analysis and acid titration for hydroxyl ion analysis [39,40]. The uncertainty of the measured ion concentrations in the pore solution is approximately 10%.

4. Experimental results

4.1. Isothermal conduction calorimetry

Fig. 1 shows heat flow profiles for the cement paste mixtures. It is seen that the hydration of the mixtures containing SRA is retarded compared to the control (plain) mixture as indicated by the rightward shift and the reduction in maximum heat flow values [41]. This retardation has been previously attributed to the reduced alkali content in the pore solution in the presence of the SRA [42]. The reduction in the alkali concentration and pH of the pore solution results in an increase in the calcium concentration of the SRA mixture (see below), which is expected to retard C_3S hydration [43,44]. This point is corroborated by TGA and pore solution analysis which indicates slower C_3S dissolution in the SRA mixture (Figs. 5 and 6) [42]. The retardation in the SRA mixture may also be in part due to delayed C_3A dissolution, due to the lower alkali-content in the pore solution (Fig. 6 and [45]). The retardation in hydration induced by the addition of the SRA, results in a degree of hydration at 48 h of 43% for SRA mixture as assessed by isothermal calorimetry, which is around 5% lower than the plain mixture.

4.2. Autogenous deformation measurements of cement pastes

Fig. 2 shows measurements of autogenous deformation zeroed to the time of final set (determined using the Vicat needle) as a function of specimen age for the cement pastes [10–12]. While the plain paste shows a plateau in shrinkage shortly after set, followed by monotonic shrinkage, the SRA paste undergoes an expansion which persists until 24 h, after which the system shrinks continuously. This does not suggest that no expansive processes are occurring in the plain paste as the measured deformation is the cumulative response of expansive and shrinkage processes. This is confirmed by the presence of the plateau for the plain mixture which indicates this mixture does indeed experience expansive processes, but their effects are negated by shrinkage. It is also noted, that the addition of the SRA results in a reduction in shrinkage of around 60% at 7 days, as compared to the control mixture. Other studies have shown that the magnitude of the expansion and the extent of shrinkage reduction depend on the chemistry of the cement and the SRA dosage [13,46].

It was additionally confirmed that the expansion in the SRA paste was not due to bleeding, wherein, the re-absorption of bleed water results in reduced shrinkage [47–49]. By measuring the amount of bleed water accumulated on the specimen surface with a syringe provided with a needle after 1, 2 and 4 h of sealed curing it was determined that both pastes had negligible bleed water which ensured, the 'design w/c' was not altered and thus the reabsorption of bleed water would not produce spurious results. Further, by measuring the temperature inside the tubes during the experiment, it was determined that the peak temperature change in the sample was around ±1 °C; so, effects due to thermal deformations can also be neglected [50,51].

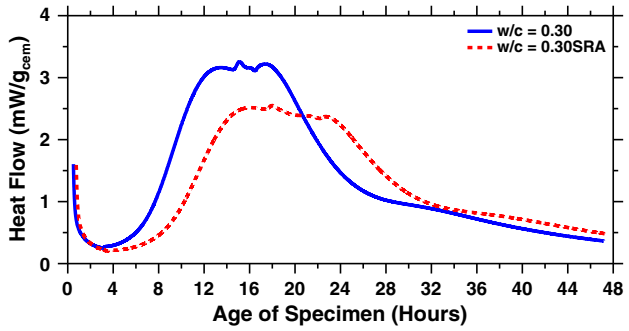

Fig. 1. Heat flow as a function of specimen age assessed for cement pastes. Measurements performed on duplicate paste specimens are observed to overlap each other.

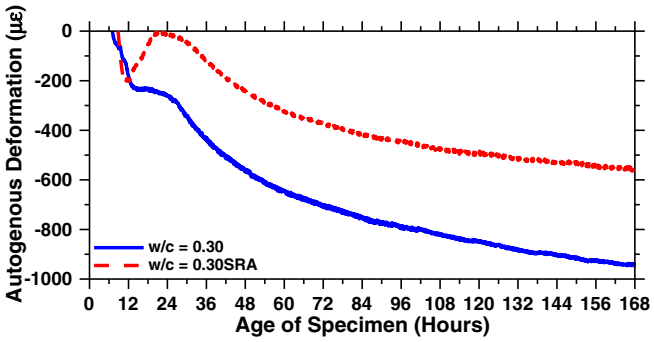

Fig. 2. Autogenous deformation as a function of specimen age for cement pastes [10–12].

4.3. Thermogravimetric (DTG) analysis of cement paste mixtures

Fig. 3 shows differential thermogravimetry (DTG) profiles for the mixtures with and without SRA at 11, 26 and 48 h after casting. After 26 h, both mixtures show similar types and quantities of hydrates in the system. However, significant differences are observed between these systems at 11 h. The plain paste shows 3 discrete peaks corresponding to the loss of evaporable water from the C–S–H, ettringite and gypsum (60–200 °C), portlandite (400–450 °C) and calcite (500–700 °C) decomposition, while the SRA paste shows an additional peak which appears around 300 °C and a smaller portlandite decomposition peak.. This is similar to results presented by Maltese et al. who noted a smaller portlandite content, at early-ages, in SRA mixtures using thermal analysis [52]. However, as seen in Fig. 4, within the uncertainty of the TGA and XRD determinations, this difference is not very significant.

From experiments on mature mortars (6 months old) with and without SRA it was deduced that the peak observed around 300 °C in the SRA pastes corresponds to the thermal decomposition of the SRA; and not hydrogarnet, AFm phases or nano-portlandite which may decompose at similar temperatures [53–55]. The area under this peak decreases with increasing age. Finally, results from another recent study suggest that the fourth peak observed around 800 °C in the SRA paste, which increases with time (hydration), corresponds to the incorporation of the SRA in the C–S–H which alters its structure, resulting in the observed decomposition pattern [56].

4.4. Quantitative X-ray diffraction using Rietveld refinement

Fig. 4 shows ettringite and portlandite contents as a function of specimen age for the plain and SRA mixtures. Within the error of the XRD measurements, both paste mixtures show similar portlandite contents at an equal age, and as such, this observation does not contradict the TGA determinations [25]. Further, at an equal age the SRA paste shows a marginally higher amount of ettringite as compared to the plain system. As such, the similar quantities of portlandite and ettringite noted in these systems do not provide clear evidence which indicates the nature of the solid phase that induces expansive deformations in the SRA system.

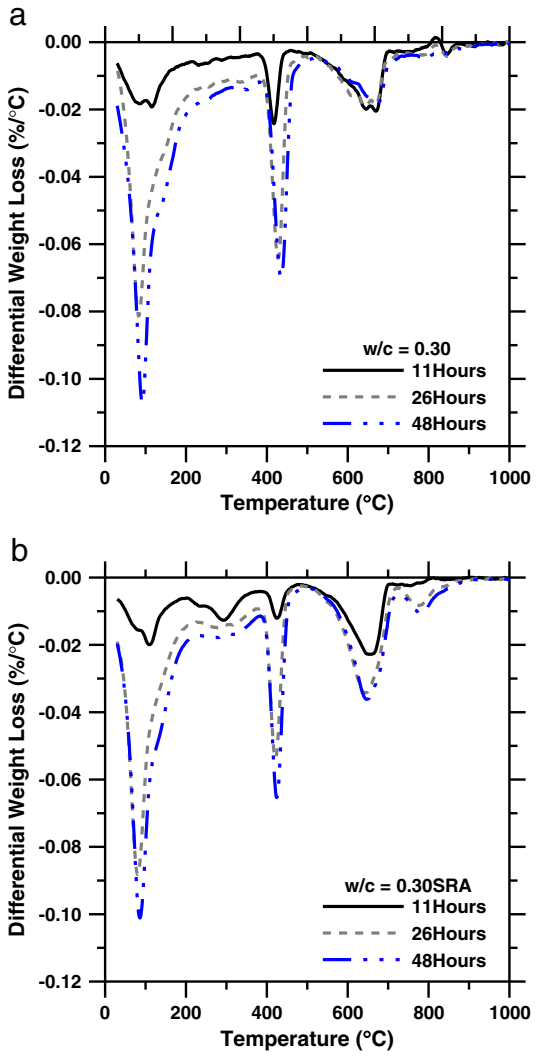

Fig. 3. Differential weight loss of cement pastes: (a) $w/c = 0.30$ and (b) $w/c = 0.30$SRA.

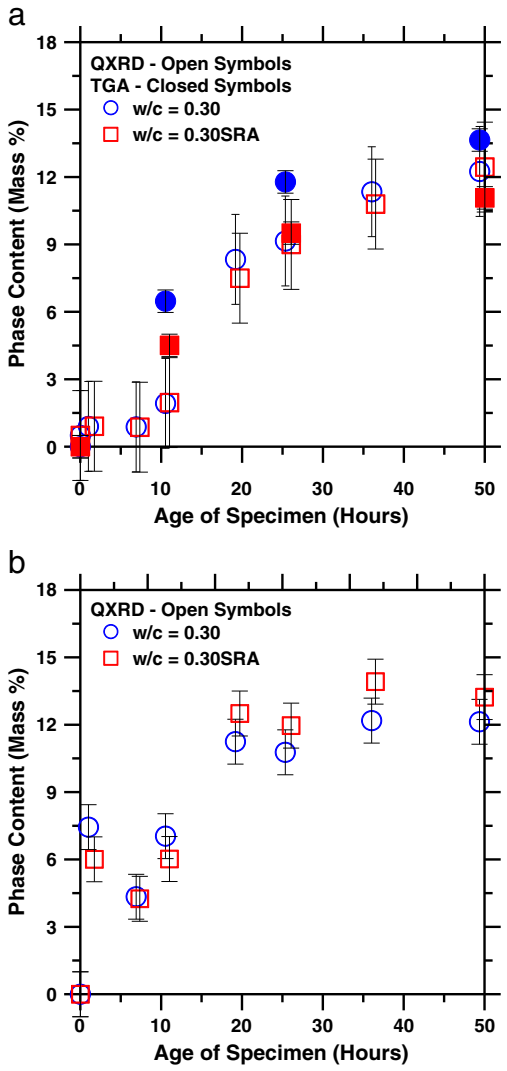

Fig. 4. The phase content as a function of age for the pastes: (a) portlandite and (b) ettringite.

4.5. Scanning electron microscopy of cement pastes

Fig. 5 shows BSE micrographs of the plain and SRA pastes at 26 h. An aspect which is clearly seen in these images is the presence of large crystals of portlandite which appear as long parallel striations in the image. This is important as these portlandite crystals have a considerably different morphology to crystals that are traditionally seen in cement pastes, which are smaller, and show a more equiaxed form [57]. The altered morphology of portlandite is most likely caused due to the adsorption-or-absorption of the superplasticizer on specific crystal-faces (001 face for portlandite) which results in preferential crystal growth in certain directions [57–60]. The altered morphology is not a consequence of the SRA as non-ionic surfactants (such as this SRA) have been found to not interact with the cement hydrates [71]. While both systems show similar portlandite crystals, there appear to be fewer such crystals in the plain paste at 11 h; in agreement with the lower saturation index of portlandite in this system (refer to Section 5.1).

4.6. Chemical compositions of expressed pore solutions

Fig. 6(a) shows the cation concentrations (K^+, Na^+, Ca^{2+}) as a function of age for the plain and SRA containing paste mixtures. The plain mixture ($w/c = 0.30$) shows higher alkali ion (K^+, Na^+) concentrations as compared to the SRA mixture ($w/c = 0.30$SRA) [42]. In contrast, the SRA mixture has a consistently higher Ca^{2+} concentration compared to the plain mixture.

Fig. 6(b) shows the anion (SO_4^{2-}, OH^-) concentrations in the paste mixtures. Initially, the plain mixture shows a higher (but constant) SO_4^{2-} concentration as compared to the SRA mixture. This difference persists until a critical point is reached (i.e., while solid gypsum is available in the system), at around 14 and 20 h for the plain and SRA mixtures respectively [61,62]. After this point, the SO_4^{2-} concentration in solution reduces monotonically and both systems show similar SO_4^{2-} contents. In contrast, the OH^- concentrations of both mixtures are similar until these critical points, after which the OH^- concentration of the plain mixture increases and remains consistently higher than that of the SRA mixture. The SRA mixture shows an increase in the OH^- concentration at a later age due to retarded hydration. The increase in the OH^- concentration corresponds, first, to the decrease in the SO_4^{2-} content after the depletion of solid gypsum and second, to an increase in the alkali contents probably due to the renewed reaction of C_3A.

Before the critical point, the pore solution's composition is buffered by the presence of solid gypsum so that the higher SO_4^{2-} concentration of the plain mixture results in a depressed Ca^{2+} concentration. After the critical point, the ion balance depends more on the presence of solid calcium hydroxide and now the higher OH^- concentration (i.e., solution pH) of the plain mixture results in a lower

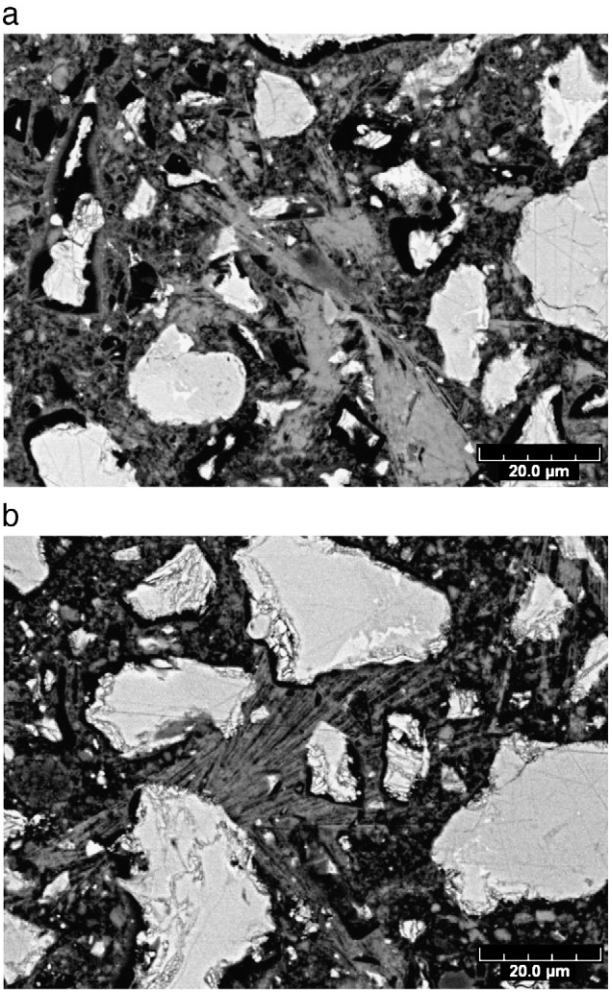

Fig. 5. Representative BSE micrographs of cement pastes at 26 h showing elongated portlandite crystals for: (a) $w/c = 0.30$ and (b) $w/c = 0.30$SRA.

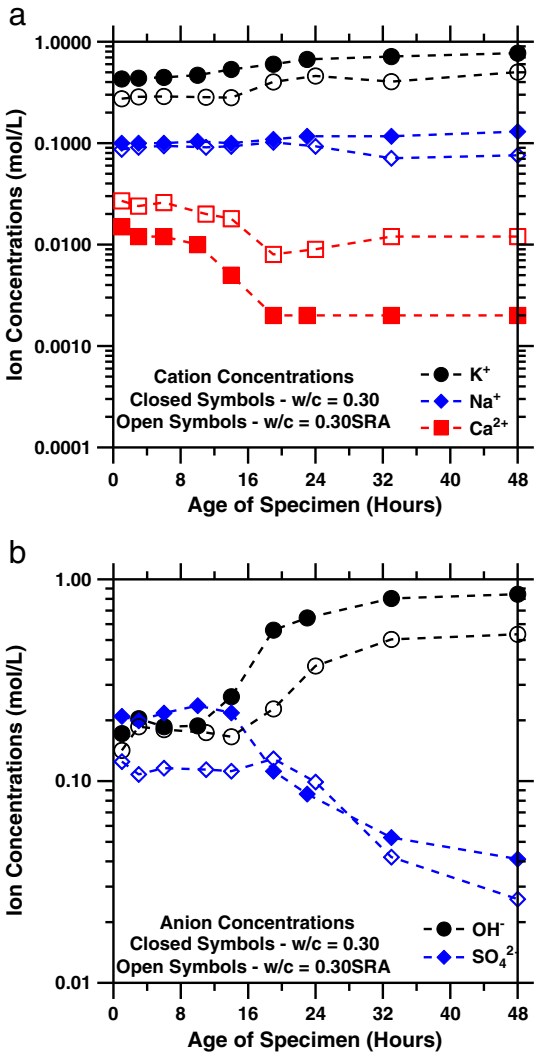

Fig. 6. The ion-composition of the expressed pore solutions as a function of specimen age for: (a) cations and (b) anions [42].

Ca^{2+} concentration. Both before and after the critical point, the higher alkali content of the plain mixture increases the concentration of the counterbalancing anion in solution (SO_4^{2-} followed by OH^-) which acts to depress the Ca^{2+} concentration, while the lower alkali-ion concentration of the SRA mixture elevates Ca^{2+} concentrations [63].

5. Discussion of experimental results

5.1. The influence of the pore solution chemistry on the effective phase saturation index

Solubility calculations were carried out using the measured concentrations of the pore solution to calculate the saturation indices of solid phases in the system. Cement paste pore solutions contain various ionic species, including single ions such as (K^+, OH^-, etc) and ion–ion pairs such as ($CaOH+$, KSO_4^-, etc.). A computational geochemical code, GEMS-PSI, was used to calculate aqueous speciation and ion-activity coefficients considering five measured species (K^+, OH^-, Na^+, Ca^{2+}, SO_4^{2-}) in the pore solution (Fig. 6) [64,65]. From analysis of the expressed pore solutions, it was noted that the solution was not exactly electro-neutral (charge-balanced). This error was always within about 6%, which is within the uncertainty of the methods used for pore solution analyses. To ensure electro-neutrality, an adjustment was made in the OH^- ion concentrations of the extracted pore solutions. In this study, the concentrations of silicate ($H_2SiO_4^-$) and aluminate ($Al(OH)_4^-$) species were not measured. For calculation of the ettringite-and-monosulfate saturation index the aluminate ion concentration was assumed equivalent to that determined for similar systems; $5 \cdot 10^{-6}$ mol/L [66].

The individual ion-activity coefficients were calculated using the Truesdell–Jones formulation of the extended Debye–Huckel equation as implemented in GEMS-PSI which is applicable for electrolytes with an ionic strength up to 2.0 mol/L [67]. The level of saturation of the pore solution with respect to the different solid phases was determined using the Effective Phase Saturation Index (SI), a function of the phase specific ion-activity and the solubility products respectively (Eq. (1) and Table 2):

$$SI = \frac{\log\left(\frac{IAP}{K_{SP}}\right)}{N} \tag{1}$$

where: IAP is the ion-activity product of the phase of interest calculated from the measured concentrations, K_{SP} is the theoretical solubility product of the same phase at equilibrium in an aqueous medium (assumed to be water at 298.15 K) and N is the number of ionic species participating in the dissolution or precipitation reaction (unitless). The effective saturation index is used (as opposed to the traditional saturation index) to account for the differing number of ions participating in a specific dissolution–precipitation process.

Table 2
Thermodynamic information for the solid phases investigated [64,72–75].

Solid phase	Ion activity product (IAP)	Solubility product at 25 °C, 1 bar (log K_{sp})	Molar volume (cm^3/mol)	Number of participating species (N)
Gypsum	$(a_{Ca}^{2+})\ (a_{SO_4^{2-}})\ (a_{H_2O})^2$	−4.58	75	2
Portlandite	$(a_{Ca}^{2+})\ (a_{OH-})^2$	−5.20	33	3
Ettringite (AFt)	$(a_{Ca}^{2+})^6\ (a_{Ca}^{2+})\ (a_{SO_4^{2-}})^3\ (a_{Al(OH)4-})^2\ (a_{OH^-})^4\ (a_{H2O})^{26}$	−44.90	707	15
Monosulfate (AFm)	$(a_{Ca}^{2+})^4\ (a_{SO_4^{2-}})\ (a_{Al(OH)_4^-})^2\ (a_{OH^-})^4\ (a_{H_2O})^6$	−29.26	309	11

It should be noted that the SI calculations are accurate only within: (1) the resolution of the methods used for cation/anion determinations, and (2) the value of the solubility product used. Further, some doubt exists regarding complexation of the SRA with ions in solution as this may result in a spurious interpretation of the saturation index. However, given the non-ionic nature of the SRA, it is expected the SRA does not appreciably form ion-complexes and the calculated SI is an accurate description of the constitution of the pore solution [68]. Further, to check any influence of electrostatic interactions caused due to the SRA the zeta potential of slurries with and without a SRA was measured [69]. These results and other polymer adsorption measurements indicate that non-ionic surfactants (such as this SRA) do not appear to significantly adsorb onto cement particles-or-hydrates or alter their zeta potential [70,71]. As such, the SRA is not expected to alter electrostatic interactions in the system [70,71].

Positive values of the saturation index indicate oversaturation, while a negative value indicates undersaturation with respect to a solid phase. The saturation index indicates the direction of progression of a reaction, i.e., precipitation for SI>0, dissolution for SI<0 and at equilibrium, SI = 0, the rate of dissolution is equivalent to the rate of precipitation. However, the SI is only a thermodynamic parameter and gives no information on the kinetics of the reaction. For example: if a reaction is kinetically restrained a solution can remain under-or-oversaturated without dissolution-or-precipitation for a long duration. As such, the SI trends are most useful to compare the level of saturation of phases in different systems. Since small departures from equilibrium are difficult to quantify exactly, they can be considered to be at equilibrium (SI = 0).

Fig. 7 shows the saturation indices for phases including ettringite, gypsum, portlandite and monosulfate in the plain and SRA mixtures. In the case of ettringite and monosulfate, while the plain mixture shows a monotonic decrease in the SIs, the SRA mixture shows a decreasing SI until approximately 20 h after which the SI once again begins to increase. Further, the SRA mixture becomes under-saturated with gypsum later due to the retardation in hydration.

The most interesting trends in the saturation indices are observed in the case of portlandite. These show very different behaviors in the two systems. In the plain system, the pore solution is initially oversaturated with portlandite until 6 h. After 6 h and until the depletion of gypsum at 14 h, portlandite is close to equilibrium. After 14 h, the solution becomes again oversaturated with portlandite. In contrast, the SRA mixture shows oversaturation with portlandite throughout the observed 48 h. Here, the higher levels of saturation for portlandite in the SRA system are related to the reduced alkali and SO_4^{2-} concentrations and the increased Ca^{2+} concentrations in solution [42,76]. Both ettringite and portlandite have higher oversaturations in the SRA system compared to the plain system in the period where the expansion occurs and therefore both phases could potentially contribute to inducing an early-age expansion due to the crystallization pressure that develops.

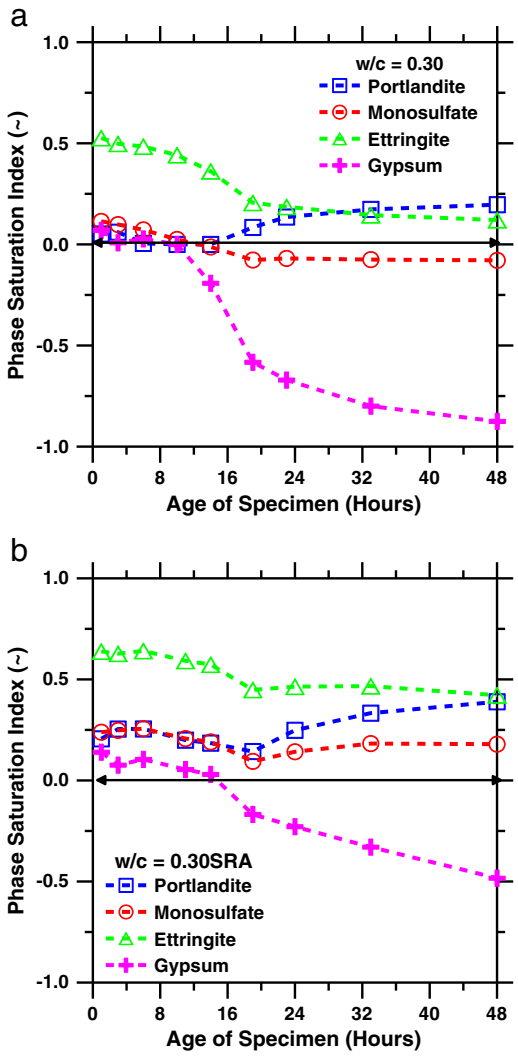

Fig. 7. The effective saturation index (SI) as a function of specimen age for the solid phases calculated using the measured pore solution chemistries: (a) $w/c = 0.30$ and (b) $w/c = 0.30$SRA. The solid line indicates equilibrium conditions (SI = 0).

5.2. The influence of the phase saturation index on the crystallization pressure

The growth of a crystal in a oversaturated solution can be related to the hydrostatic pressure required to be applied on the crystal to prevent it from growing using Eq. (2) [77–80]:

$$\sigma_C = \frac{RT}{\nu_M} \cdot ln\left(\frac{IAP}{K_{SP}}\right) \quad (2)$$

where: σ_C is the hydrostatic pressure exerted on the crystal (MPa), R is the universal gas constant (8.314 J/K mol), ν_M is the molar volume of the crystal (cm^3/mol), T is the thermodynamic temperature (296.15 K), IAP is the ion-activity product of the phase and K_{SP} is the solubility product of the phase of interest in the aqueous medium (assumed to be water). Here, the ratio IAP/K_{SP} describes the saturation level of a phase in solution in its traditional form without accounting for the number of participating ions in solution, as in this case the normalization is ensured by the molar volume term (ν_M).

Fig. 8 shows the hydrostatic pressure exerted by the crystals (σ_C) for portlandite and ettringite where the relevance of the oversaturation level to the pressure is clearly seen. For ettringite, in the period corresponding to the initiation of the expansion, the pressure is

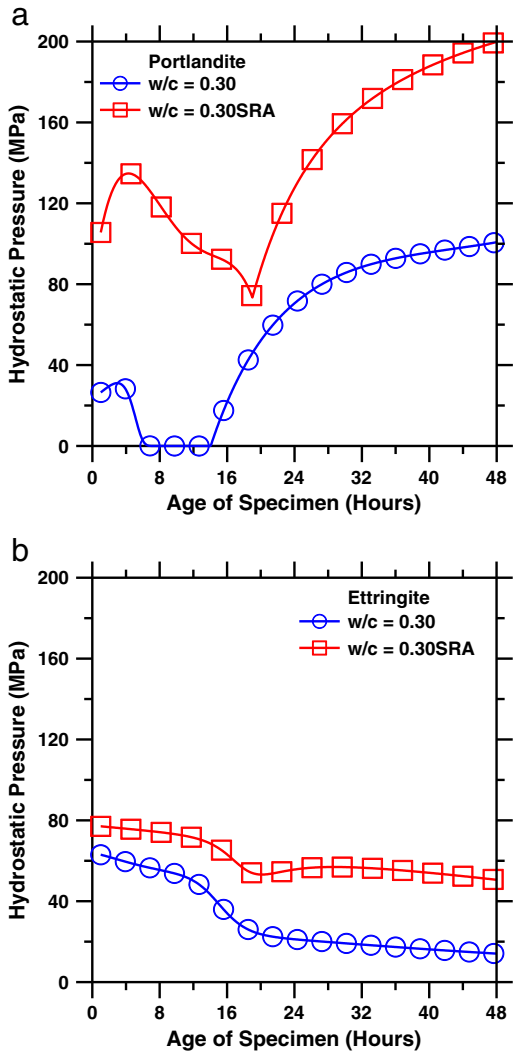

Fig. 8. The hydrostatic pressure applied on the crystal as a function of specimen age for: (a) portlandite and (b) ettringite. Here only positive pressures, corresponding to oversaturation with respect to the solid phase in the pore solution are shown[5].

similar in the plain and SRA systems. However, for portlandite the lower saturation in the plain system leads to a much larger difference in the calculated pressures during the same time-period (Fig. 8a). The expansive pressures then obviously follow the trends in the SIs which indicates that while the crystallization stresses associated with ettringite diminish with time, expansive stresses related to portlandite increase with time [81,82]. This is an important point which downplays the role of ettringite as the main cause of expansion in the cement paste systems examined in this study.

Using a poromechanical formulation, the expansive stress developed in a pore can be related to the volume fraction of the crystalline phase (occupying the porosity) exerting a stress and the pressure applied on the crystal to prevent it from growing as shown in Eq. (3) [83,84]:

$$\sigma_{EC} = \sigma_C \cdot S_C = \sigma_C \cdot \left(\frac{R\phi_C}{\phi_T}\right) \tag{3}$$

[5] It should be noted that the absolute values of the crystallization pressure shown in Fig. 8 are likely much higher than the actual pressure that develops in the system. In the limit, the crystallization pressure developed will always be less than or equal to the disjoining pressure (which is likely much lower than the values described in Fig. 8) applied by the pore-wall (through the adsorbed water film) on the confined crystal [80].

where: σ_{EC} is the expansive hydrostatic stress developed in the body due to phase crystallization (MPa), S_C is the fraction of the pore space occupied by portlandite crystals, σ_C is the hydrostatic pressure (MPa) described in Eq. (2), ϕ_C is the volume fraction of portlandite in the overall system (fraction), R is a numerical 'phase reduction-factor' which scales the total portlandite volume in the system to the volume of portlandite which grows in the pore-spaces and causes expansions and ϕ_T is the total porosity in the system. Here, the total fluid (liquid and–or vapor; ϕ_T) filled porosity of the system was computed using Powers model and the extent of hydration determined using isothermal calorimetry measurements assuming the system begins to desaturate (i.e., self-desiccate) at final set [90,91].

Through Eq. (3), it can be inferred since the quantity of portlandite and ettringite is similar (Fig. 3), the majority of expansive stresses in the SRA system are caused due to portlandite crystallization as dictated by the difference in the saturation level in the pore solution. As such, the volume fraction of portlandite was computed as a function of the degree of hydration of the cement assuming in the first 48 h, portlandite is produced mainly by alite hydration. This is reasonable given the small contribution of belite hydration at early ages (i.e., QXRD data suggests only around 2% of the belite has reacted in the first 48 h [70,85]). This calculation assumes 1.00 volume unit of alite on complete reaction with water produces 0.59 volume units of portlandite, for a Ca/Si ratio of 1.7 of the C–S–H for a sealed, hydrating system.

Eq. (3) assumes that the entire volume of the expansive phase is restrained by the cavity and is capable of generating an expansive stress. This is obviously inaccurate as often, crystals can grow unrestrained in a pore space without exerting an expansive stress. Here, it is assumed that 12.5% (i.e., $R = 0.125$) of the portlandite crystals (e.g., growing in the smallest pores where the largest stresses develop) exert an expansive stress, as this value was determined to generate the best-replication of the experimental results. While the authors do acknowledge that this assumption is arbitrary, it is made for this example since a more realistic estimate of the volume fraction of the crystalline phase exerting an expansive stress is not available at this time due to limitations imposed on experimental methods of determination. Further, it is also important to note that the expansive stresses discussed here are relevant only after the cement paste has solidified (i.e., set).

For a crystal growing into a spherical pore with cylindrical entryways, the hydrostatic pressure (σ_C) can also be related to the oversaturation level in solution and the equilibrium curvature of the crystal–liquid (solid–liquid) interface as described using Eq. (4) [77,79]:

$$\frac{2\gamma_{SL}}{r} = \frac{RT}{v_M} \cdot ln\left(\frac{IAP}{K_{SP}}\right) \tag{4}$$

where: γ_{SL} is the interfacial (crystal–liquid) surface energy (assumed 0.1 N/m at the portlandite–water interface, [86]) and r is the equilibrium curvature (radius) of the crystal at its tip (m). Here, the crystal–liquid surface energy is used as an effective interfacial energy applicable to the entire crystal surface without considering the specific variations in interfacial energy along different crystal faces (planes) [77]. By combining Eqs. (2) and (4) it is possible to conclude that the saturation level of a phase in solution is directly proportional to the hydrostatic pressure applied on the crystal and inversely related to the radius of the crystal at its tip (decreasing radius with increasing saturation). This is important as in the case of the SRA mixture, the higher portlandite saturation is expected to initially nucleate and grow crystals of a smaller size (radius) than the plain mixture [87]. For example: in the case of portlandite, the radius at the crystal-tip in the SRA system is calculated to be between 2 and 50 times smaller than the plain system and in the range of 2–3 nm. Recent observations of cement pastes containing another organic

admixtures do also suggest the presence of such nano-portlandite inter-mixed in the C–S–H as determined from the elevated Ca/Si ratio as measured using SEM-EDS analysis [88].

5.3. The influence of crystallization stresses on early age deformations

Early-age autogenous deformations are a competitive process between expansions resulting from crystallization pressures generated due to solid phase formation and shrinkage resulting from the effects of chemical shrinkage and capillary depression (vapor space expansion). This competitive mechanism can be mathematically generalized using Eq. (5):

$$\varepsilon_{AD} = f(\sigma_{EC}, \sigma_{RH}) \tag{5}$$

where: ε_{AD} is the net autogenous (sealed) deformation experienced by the material (expansion or shrinkage), σ_{EC} is the expansive (positive) crystallization stress developed in the system and σ_{RH} is the tensile (negative) shrinkage stress that develops due to self-desiccation. Consequently, autogenous deformations in cementitious materials can be modeled by quantifying the expansive stresses generated due to phase crystallization under conditions of solution oversaturation and tensile stresses induced in the pore solution due to water consumption during hydration (self-desiccation) which draw the pore walls closer together and induce shrinkage.

The formation of empty-vapor spaces due to chemical shrinkage and the consumption of water during hydration results in a depression of the internal equilibrium relative humidity (and the degree of fluid saturation) in the pores [10,89]. The measured internal humidity (Fig. 9c) is influenced by the presence of dissolved species, which act to depress the relative humidity (RH) as described by Raoult's Law, where the RH depression is a function of the ionic-strength of the pore fluid (increasing RH depression with increasing ionic strength) and the curvature of the interfacial meniscus (liquid–vapor) that forms due to water consumption during hydration as described using Kelvin's Law (Eq. (7) [10]. As such, the measured relative humidity (RH_M) in the pore-structure can be described as shown in Eq. (6):

$$RH_M = a_W \cdot RH_K \tag{6}$$

where: RH_M is the measured internal relative humidity (fraction), a_W is the ionic-strength dependent activity of the water in the pore solution; the Raoult effect (fraction) and RH_K is the contribution to the relative humidity due to the consumption of the pore-fluid during hydration (or drying), the Kelvin effect (fraction). In this study, the activity of the water present as pore solution calculated using the pore solution composition and the SRA content in solution and the measured relative humidity(RH_M) were used to compute the direct effect of meniscus formation on relative humidity depression (RH_K) [10,89]. This approach enables estimation of the capillary pressure developed in the pore-fluid independent of the ionic strength of the pore solution, the solution surface tension and the pore-geometry as shown in Eq. (7) [10,89]:

$$\sigma_{RH} = -\frac{ln(RH_K)RT}{V_M} \tag{7}$$

where: σ_{RH} is the suction pressure (MPa) developed in the pore-fluid due to the effects of relative humidity depression (self-desiccation), R is the universal gas constant (8.314 J/Kmol), T is the thermodynamic temperature (296.15 K) and V_M is the molar volume of the pore fluid (assumed to be water, 18.02 cm^3/mol).

Consequently, the effective stress developed in the pore-structure can be expressed as the difference between the expansive stress developed due to crystallization and the capillary stress developed due to RH depression as shown in Eq. (8) and Fig. 9(a) [83,84]:

$$\sigma_E = \sigma_{EC} - \sigma_{RH} \cdot S_L \tag{8}$$

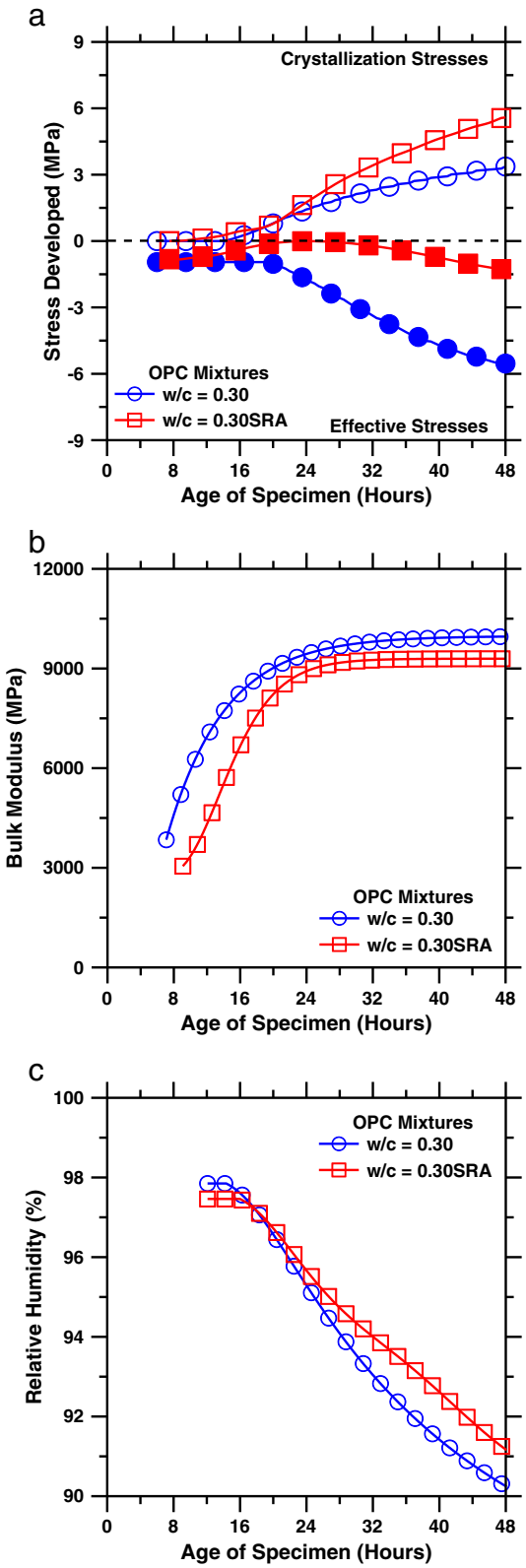

Fig. 9. (a) The crystallization and effective stresses developed in the microstructure, (b) the bulk modulus (K_b) of the plain and SRA containing cement pastes [92] and (c) The measured relative humidity as a function of specimen age for the plain and SRA containing pastes [10,11].

where: σ_E is the effective stress developed in the material (MPa); that is the difference between the hydrostatic expansive stress developed due to portlandite crystallization (σ_{EC}) and the shrinkage stress

developed due to capillary depression (σ_{RH}) and S_L is the degree of liquid saturation of the body calculated Powers model and the extent of hydration measured using isothermal calorimetry assuming the system begins to self-desiccate at final set [90,91].

The effective stress (σ_E) developed can then be combined with the elastic properties to compute the net deformation experienced by the material using Eq. (9) [93,94]. It should be noted, Eq. (9), as originally formulated is strictly applicable only for fully-saturated, linear-elastic materials and its validity in the case of partial saturation is only approximate [93,94]:

$$\varepsilon_{LIN} = \left(\frac{\sigma_E}{3}\right)\cdot K \tag{9a}$$

$$K = \left(\frac{1}{K_B} - \frac{1}{K_S}\right) \tag{9b}$$

where: ε_{LIN} is the linear deformation experienced by the material (με), σ_E is the effective stress developed in the material (MPa), K is a term that represents the time dependent evolution of elastic properties in the material (GPa^{-1}), K_B is the bulk modulus of the partially saturated cement paste including the effects of porosity (GPa) and K_S is the bulk modulus of the solid-skeleton excluding the effects of the porosity (assumed constant; 44 GPa, [95,96]). The bulk modulus of the cement pastes (Fig. 9b; K_B) was calculated using ultrasonic wave-speeds measured in through-transmission mode assuming a constant Poisson's ratio ($\nu = 0.22$) [92,97].

To account for the evolution of properties in the cement paste with time and hydration (aging), Eq. (9a) can be written in an incremental form as shown in Eq. (10a):

$$\Delta\varepsilon(t)_{LIN} = \left(\frac{\Delta\sigma_E(t)}{3}\right)\cdot K + \left(\frac{\sigma_E}{3}\right)\cdot \Delta K(t) \tag{10a}$$

where: $\Delta\sigma_E(t)$ is the incremental change in the effective stress in the pore structure (MPa) over a given time period and $\Delta K(t)$ is the incremental change in the elastic properties of the material (MPa^{-1}) over a given period. The net deformation experienced by the paste is calculated by integrating Eq. (10a) over a specific time interval as shown in Eq. (10b):

$$\varepsilon_{LIN}(t) = \sum_{t=0}^{t=t}\left(\frac{\Delta\sigma_E(t)}{3}\right)\cdot K + \sum_{t=0}^{t=t}\Delta K(t)\cdot\left(\frac{\sigma_E}{3}\right) \tag{10b}$$

Fig. 10 shows normalized results of the measured and computed autogenous deformation as a function of specimen age for the plain ($w/c = 0.30$) and SRA ($w/c = 0.30$SRA) mixtures. The simulation replicates the shape (form) of the experimental measurements over time as shown in Fig. 10 (c and d). Here, the calculated deformation for the plain mixture shows a plateau in shrinkage shortly after the time of set followed by monotonic shrinkage similar to the measured response. This is also consistent for the SRA mixture which begins expanding around 12 h and expands until 24 h, followed by monotonic shrinkage similar to the measured response.

However, the calculations do not well capture the true magnitude of the deformations, which is about 3 and 6 times less than the measured value at 48 h for the plain and SRA mixtures respectively as shown by the deformation curves plotted on an unnormalized scale; Fig. 10 (a and b). The discrepancies observed in the measured and calculated autogenous deformation may be attributed to a variety of factors including:

- A considerable discrepancy in the measured and modeled deformation results seems to arise from an underestimation of the shrinkage stress developed. This may be related to difficulties such as condensation on and–or drift of the *RH* sensors which may affect measurements of internal *RH* at high levels at early ages. Second, the *RH* and pore solution measurements assess the global state of the system. At a local scale, the actual *RH* may be lower leading to an underestimation of the shrinkage that develops. Further, uncertainties in the measurement of the bulk modulus (K_B) which evolves rapidly at early-ages would further limit the accuracy of the modeling approach [98].
- There exists considerable uncertainty in determination of the fraction of the crystalline phase that is able to exert an expansive stress due to pore-size (and geometry) and local solution oversaturation considerations. As such, unless the crystal is restrained by the pore-walls it will grow without exerting a stress and the local oversaturation will drop as the crystal grows by drawing ions from the solution which are replenished by diffusion from other locations or local dissolution to maintain equilibrium. Thus, the crystallization pressure would be overestimated if the solution is no longer saturated and the crystal does not grow or if the crystal does not touch the pore walls. Also, the geometry of the pores and the crystal and the effect of the confining pressure of the pore-walls on the solubility of the crystal are not considered in this analysis [77,99]. This highlights a need to account for dissimilar effects relevant to the pore-size distribution, pore connectivity, pore and crystal geometry to precisely analyze crystallization-and-shrinkage stresses that may be expected to develop in the system.
- The approach used to model autogenous deformations is of a strictly linear elastic nature. As such, it does not incorporate viscoelastic (i.e., creep and strain-rate) effects which may be significant at early-ages. In addition, the analysis upscales the crystallization and shrinkage stresses to the global scale. As a result, crystallization and self-desiccation as occurs in small or disconnected pores may not be appropriately considered in the analysis. This is important as capillary-and-crystallization stresses are most crucial at the scale of the smallest pores. Both these points may in part explain the underestimation of the calculations [89]. Further, the modeling approach neglects effects arising from hydrate dehydration induced due to self-desiccation [100]. As such, a continuous reduction in the 'moisture-level' of the C–S–H (i.e., aging) and the other reaction products as occurs during cement hydration would be another contribution which may explain the underestimation of the calculations. Finally, changes in the fluid saturation level or elastic properties that occur due to the volume change of the pores during expansion or shrinkage are also not accounted for in the calculations [101].

However, inspite of the mismatch in the magnitude of the experimental results and calculated deformation, the results are useful in that they depict the effects of crystallization stress driven early-age deformations in cementitious materials.

6. Summary and conclusions

This paper assesses the early-age autogenous deformation behavior of cement pastes containing a shrinkage reducing admixture (SRA). Experimental measurements of autogenous deformation, electron microscopy and solid and liquid phase analysis have been integrated with calculations of the effective saturation indices to understand the chemical nature of the early-age expansion. For the cement chemistry and SRA evaluated, the results suggest that, for the SRA mixture, the amplification in portlandite oversaturation and its crystallization causes an early-age expansion.

The pore solution saturation level has been related to the size of crystals and the magnitude of crystallization stresses that may be expected to develop in the material. An effort has been made to model crystallization stress driven expansions in cementitious materials. The modeling results are useful in replicating the temporal form (shape) of the experimental response and conceptually illustrating the effect of crystallization stresses on deformations. This research has

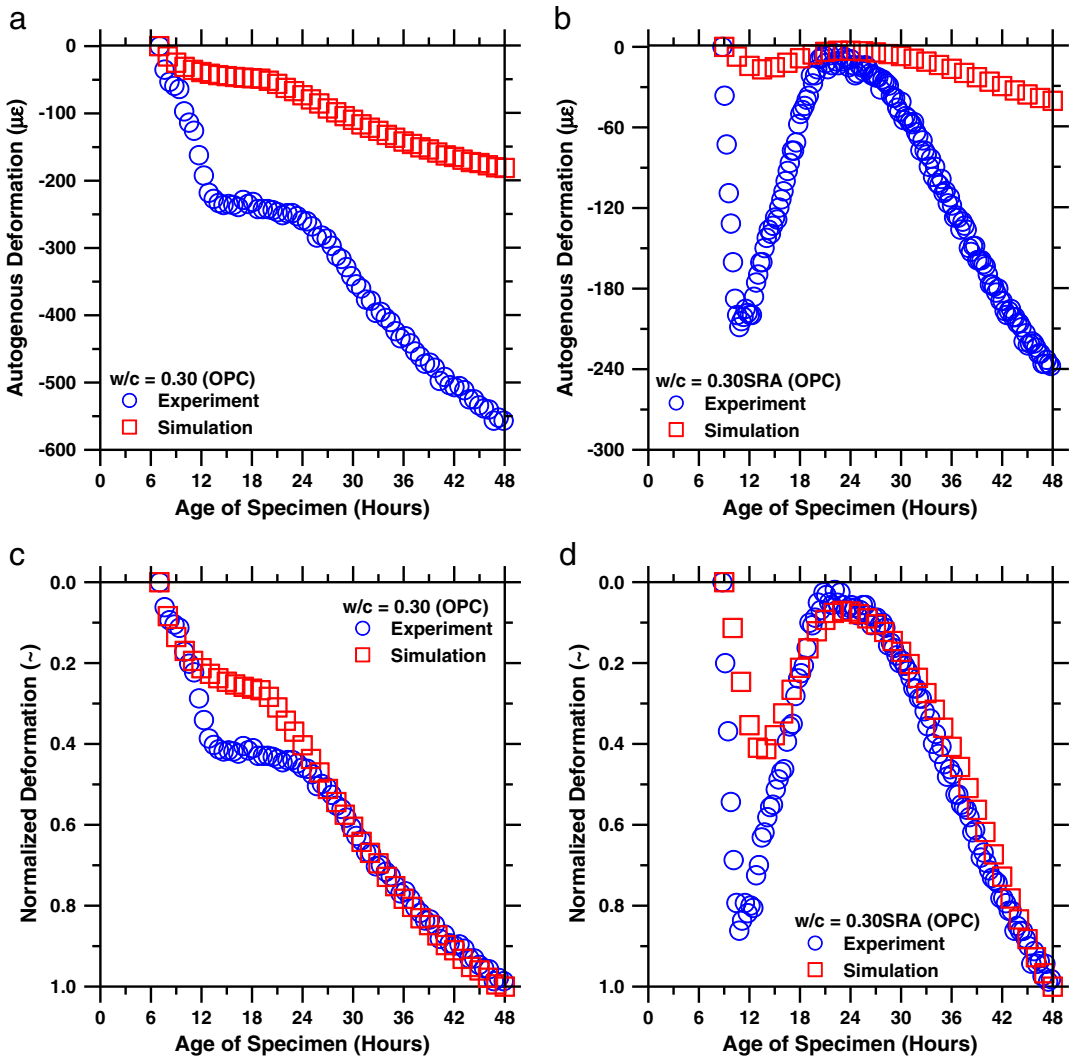

Fig. 10. The measured and calculated autogenous deformation as a function of specimen age for the plain and SRA cement pastes on: (a and b) actual scale and (c and d) normalized scale.

implications on understanding the shrinkage and shrinkage-cracking behavior of concretes containing SRAs. This is especially relevant in the case of producing concretes that generate a specific level of expansion and resist cracking and–or developing material inputs for computer models that aim to simulate volume changes or the risk of cracking in concretes containing SRAs.

Acknowledgements

The authors gratefully acknowledge the financial support for this research which has come from the Purdue Research Foundation. This research was conducted in the Materials Characterization and Sensing Laboratory at Purdue University, the Laboratory of Construction Materials at the Ecole Polytechnique Federale de Lausanne and the Laboratory for Concrete and Construction Chemistry at the Swiss Federal Laboratories for Materials Testing and Research. As such, the authors gratefully acknowledge the support of these laboratories in making this research possible. The authors would also like to acknowledge Dale Bentz (NIST), George Scherer (Princeton University) and Pietro Lura (EMPA) for extended insightful discussions and valuable comments that helped to greatly improve this paper. The contents of this paper reflect the views of the authors, who are responsible for the accuracy of the data presented herein.

References

[1] M. Shoya, S. Sugita, T. Sugiwara, Improvement of drying shrinkage and shrinkage cracking of concrete by special surfactant, in: E. Vázquez (Ed.), Admixtures for concrete: improvement of properties, Chapman and Hall, London, 1990, pp. 484–495.
[2] A. Balogh, New admixture combats concrete shrinkage, Aberdeen's Concrete Construction 41 (7) (1996) 546–551.
[3] C. Nmai, R. Tomita, F. Hondo, J. Buffenbarger, Shrinkage reducing admixtures, Concrete International 20 (4) (1998) 31–37.
[4] N.S. Berke, M.C. Dallaire, M.C. Hicks, A. Kerkar, New developments in shrinkage-reducing admixtures, superplasticizers and other chemical admixtures in concrete, Proceedings Fifth CANMET/ACI International Conference, 1997, pp. 971–988, Rome, Italy.
[5] S.P. Shah, W.J. Weiss, W. Yang, Shrinkage cracking – can it be prevented? Concrete International 20 (4) (1998) 51–55.
[6] H. Ai, J.F. Young, Mechanisms of shrinkage reduction using a chemical admixture, in: H. Justnes (Ed.), Proceedings of the 10th Int. Cong. on the Chemistry of Cement, 1997, pp. 18–22, Gothenburg, Sweden.
[7] J. Ambroise, J. Georgin, S. Peysson, S. Pera, 'Influence of Polyether Polyol on the Hydration and Engineering Properties of Calcium Sulfoaluminate Cement', Cement and Concrete Composites 31 (7) (2009) 474–482.
[8] M. Collepardi, A. Borsoi, S. Collepardi, J.J. Ogoumah Olagot, R. Troli, Effects of shrinkage reducing admixture in shrinkage compensating concrete under non-wet curing conditions, Cement and Concrete Composites 27 (6) (2005) 704–708.
[9] S.P. Shah, M.E. Karaguler, M. Sarigaphuti, Effects of shrinkage reducing admixture on restrained shrinkage cracking of concrete, ACI Materials Journal 89 (3) (1992) 88–90.
[10] W.J. Weiss, P. Lura, F. Rajabipour, G. Sant, Performance of shrinkage reducing admixtures at different humidities and at early ages, ACI Materials Journal 105 (5) (September-October 2008) 478–486.

[11] G. Sant, F. Rajabipour, P. Lura, W.J. Weiss, Examining time-zero and early age expansion in pastes containing shrinkage reducing admixtures (SRAs), 2nd International RILEM Symposium on Advances in Concrete through Science and Engineering, RILEM, Quebec City, Canada, 2006, p. 353.

[12] Sant, G., 'Examining Volume Changes, Stress Development and Cracking in Cement Based Materials', MSCE Thesis, Purdue University, West Lafayette, IN, USA, pp. 235, (2007).

[13] D. Bentz, M. Geiker, K. Hansen, Shrinkage reducing admixtures and early-age desiccation in cement pastes and mortars, Cement and Concrete Research 31 (7) (2001) 1075–1085.

[14] P. Lura, B. Pease, G.B. Mazzotta, F. Rajabipour, W.J. Weiss, Influence of shrinkage-reducing admixtures on development of plastic shrinkage cracks, ACI Materials Journal 104 (2) (2007) 187–194.

[15] G. Sant, F. Rajabipour, P. Lura, J. Weiss, Volume changes in pastes containing shrinkage reducing admixtures under autogenous and drying conditions, Proceedings of the 12th International Congress on the Chemistry of Cement, Montreal, Canada, 2007, p. 10.

[16] D.P. Bentz, Curing with shrinkage-reducing admixtures: beyond drying shrinkage reduction, Concrete International 27 (10) (2005) 51–60.

[17] G. Sant, F. Rajabipour, P. Lura, W.J. Weiss, Examining residual stress development in cementitious materials experiencing an early-age expansion, 9th CANMET-ACI Int. Conf. – T.C. Holland Symposium, Warsaw, Poland, 2007, p. 8.

[18] D. Cusson, Effect of blended cements on efficiency of internal curing of HPC, ACI-SP 256, Internal Curing of High-Performance Concretes: Laboratory and Field Experiences, MI, 2008, pp. 105–120.

[19] ASTM Annual Book of ASTM Standards, Concrete and Aggregates, West Conshohocken, USA, 2009.

[20] Goto, T., Sato, T., Sakai, K., Motohiko, I., 'Cement-shrinkage-reducing agent and cement composition', United States Patent Number: 4547223, Nihon Cement Company Limited, Kyoto, Japan, (1985).

[21] D.P. Bentz, A three-dimensional cement hydration and microstructure program I – hydration rate, heat of hydration, and chemical shrinkage', NISTIR 5756, Department of Commerce, USA, 1995.

[22] G. Sant, P. Lura, W.J. Weiss, Measurement of volume change in cementitious materials at early ages: a review of testing protocols and interpretation of results, Transportation Research Record 1979 (2006) 21–29.

[23] O.M. Jensen, P.F. Hansen, A dilatometer for measuring autogenous deformation in hardening portland cement paste, Materials and Structures 28 (1995) 181.

[24] K.L. Scrivener, Backscattered electron imaging of cementitious microstructures: understanding and quantification, Cement & Concrete Composites 26 (8) (2004) 935–945.

[25] K.L. Scrivener, T. Füllmann, E. Gallucci, G. Walenta, E. Bermejo, Quantitative study of portland cement hydration by X-ray diffraction/rietveld analysis and independent methods, Cement and Concrete Research 34 (2004) 1541–1547.

[26] F. Nishi, Y. Takeuchi, I. Maki, TriCalcium silicate $Ca_3O(SiO_4)$: the monoclinic superstructure, Zeitschrift für Kristallographie 172 (1985) 297–314.

[27] T. Tsurumi, Y. Hirano, H. Kato, T. Kamiya, M. Daimon, Crystal structure and hydration of belite, Ceramic transactions 40 (1994) 19–25.

[28] A.A. Colville, S. Geller, The crystal structure of brownmillerite, Ca_2FeAlO_5, Acta Crystallographica 27 (1971) 2311–2315.

[29] P. Mondal, J.W. Jeffery, The crystal structure of tricalcium aluminate, $Ca_3Al_2O_6$, Acta Crystallographica 31 (1975) 689–697.

[30] W.F. Cole, C.J. Lancucki, A refinement of the crystal structure of gypsum $CaSO_4(H_2O)$, Acta Crystallographica 30 (1974) 921–929.

[31] F.C. Hawthorne, R.B. Ferguson, Anhydrous sulfates II: refinement of the crystal structure of anhydrite, Canadian Mineral 13 (1975) 289–292.

[32] D. Taylor, Thermal expansion data I: binary oxides with the sodium chloride and wurtzite structure, Journal of the British Ceramic Society 83 (1984) 5–9.

[33] H.E. Petch, The hydrogen positions in portlandite, $Ca(OH)_2$, as indicated by the electron distribution, Acta Crystallographica 14 (1961) 950–957.

[34] A.E. Moore, H.F.W. Taylor, The crystal structure of ettringite, Acta Crystallographica 26 (1970) 386–393.

[35] W.A. Dollase, Correction of intensities for preferred orientation in powder diffractometry: application of the march model, Journal of Applied Crystallography 19 (1986) 267–272.

[36] E.J. Sonneveld, J.W. Visser, Automatic collection of powder data from photographs, Journal of Applied Crystallography 8 (1975) 1–7.

[37] H.M. Rietveld, A profile refinement method for nuclear and magnetic structures, Journal of Applied Crystallography 2 (2) (1969) 65–71.

[38] Penko, M., 'Some Early Hydration Processes in Cement Pastes as Monitored by Liquid Phase Composition Measurements', Ph.D. Dissertation, Purdue University, West Lafayette, IN, (1983).

[39] R.S. Barneyback Jr., S. Diamond, Expression and analysis of pore fluids from hardened cement paste, Cement and Concrete Research 1 (2) (1984) 279–285.

[40] Barneyback, R. S., Jr., Alkali–Silica reactions in Portland Cement Concrete, Ph.D. Dissertation, Purdue University, West Lafayette, IN, USA, (1983).

[41] K.J. Folliard, N.S. Berke, Properties of high-performance concrete containing shrinkage reducing admixture, Cement and Concrete Research 27 (9) (1997) 1357–1364.

[42] F. Rajabipour, G. Sant, W.J. Weiss, Interactions between shrinkage reducing admixtures and cement paste's pore solution, Cement and Concrete Research 38 (5) (2008) 606–615.

[43] S. Garrault, A. Nonat, Hydrated layer formation on tricalcium and dicalcium silicate surfaces: experimental study and numerical simulations, Langmuir 17 (2001) 8131–8138.

[44] P. Juilland, E. Gallucci, R.J. Flatt, K.L. Scrivener, 'Dissolution Theory as Applied to Alite Hydration', Cement and Concrete Research 40 (6) (2010) 831–844.

[45] I. Jawed, J. Skalny, Alkalis in cement: a review, Cement and Concrete Research 8 (1) (1978) 37–51.

[46] Sant, G., 'Fundamental Investigations Related to the Mitigation of Volume Changes in Cement-Based Materials at Early Ages', PhD Dissertation, Purdue University, West Lafayette, IN, USA, pp. 226, (2009).

[47] P. Lura, O.M. Jensen, Measuring techniques for autogenous strain of cement paste, Portland Cement Association, PCA R&D Serial No. 2925 (Skokie, IL), 2005, p. 26.

[48] O. Bjontegaard, T.A. Hammer, E.J. Sellevold, On the measurement of free deformation of early age cement paste and concrete, Cement and Concrete Research 26 (5) (2004) 427–435.

[49] B.J. Mohr, K.L. Hood, Influence of bleed water reabsorption on cement paste autogenous deformation, Cement and Concrete Research 40 (2) (2010) 220–225.

[50] O. Bjontegaard, E.J. Sellevold, Interaction between thermal dilation and autogenous deformation in high performance concrete, RILEM Materials and Structures 34 (5) (2001) 266–272.

[51] P. Turcry, A. Loukili, L. Barcelo, J.M. Casabonne, Can the maturity concept be used to separate the autogenous shrinkage and thermal deformation of a cement paste at early age? Cement and Concrete Research 32 (9) (2002) 1443–1450.

[52] C. Maltese, C. Pistolesi, A. Lolli, A. Bravo, T. Cerulli, D. Salvioni, Combined effect of expansive and shrinkage reducing admixtures to obtain stable and durable mortars, Cement and Concrete Research 35 (12) (2005) 2244–2251.

[53] Bentz, D.P., 'Thermal Analysis of VERDICT Mortars: The Influence of Shrinkage Reducing Admixtures: Unpublished Results', Building and Fire Research Laboratory, National Institute of Standards and Technology, Maryland, USA, (2009).

[54] H.F.W. Taylor, Cement Chemistry, Thomas Telford2nd ed., 1997, p. 480.

[55] F.P. Glasser, The role of $Ca(OH)_2$ in Portland cement concretes, Chapter in Materials Science of Concrete Series, Calcium Hydroxide in Concrete, 2001, pp. 11–36.

[56] J.J. Beaudoin, H. Drame, L. Raki, R. Alizadeh, Formation and properties of C–S–H–PEG nanostructures, Materials and Structures 42 (7) (2009) 1003–1014.

[57] S. Diamond, Calcium hydoxide in cement paste and concrete – a microstructural appraisal, in: J. Skalny, J. Gebauer, I. Odler (Eds.), Materials Science of Concrete Special Volume on Calcium Hydroxide in Concrete, The American Ceramic Society, Ohio, 2000, pp. 37–58.

[58] R.L. Berger, J.D. McGregor, The influence of admixtures on the morphology of calcium hydroxide formed during tricalcium silicate hydration, Cement and Concrete Research 2 (1972) 43–55.

[59] A. Zingg, L. Holzer, A. Kaech, F. Winnefeld, J. Pakusch, S. Becker, L. Gauckler, The microstructure of dispersed and non-dispersed fresh cement pastes — new insight by cryo-microscopy, Cement and Concrete Research 38 (4) (2008) 522–529.

[60] P.E. Stutzman, J.R. Clifton, Microstructural features of some low water/solids, Silica Fume Mortars Cured at Different Temperatures, NISTIR 4790, U.S. Department of Commerce, April 1992, p. 17.

[61] S. Diamond, S. Ong, Effects of added alkali hydroxides in mix water on long-term SO_4^{2-} concentrations in pore solution, Cement & Concrete Composites 16 (1994) p. 219–226.

[62] S. Ong, S. Diamond, Unexpected effects of alkali hydroxide added to cement mix water, in: M. Moukwa, et al., (Eds.), Cement Based Materials: Present, Future and Environmental Aspects, Ceramic Transactions, 37, American Ceramic Society, 1993, pp. 37–48.

[63] M.C.G. Juenger, H.M. Jennings, Effects of high alkalinity on cement pastes, ACI Materials Journal 98 (3) (2001) 251–255.

[64] T. Matschei, B. Lothenbach, F. Glasser, Thermodynamic properties of Portland cement hydrates in the system $CaO-Al_2O_3-SiO_2-CaSO_4-CaCO_3-H_2O$, Cement and Concrete Research 37 (10) (2007) 1379–1410.

[65] Gibbs energy minimization software, http://gems.web.psi.ch, July 30 2009, last verified.

[66] Eberhardt, A., PhD Thesis (In development), (2010).

[67] D. Kulik, available at, GEMS-PSI Version 2.0, The Paul Scherrer Institute, Villigen, Switzerland, June 22, 2009, http://GEMS-PSI.web.psi.ch, last verified.

[68] M.J. Rosen, Surfactants and interfacial phenomena, 3rd ed., Wiley-Interscience, July 15 2004, p. 464, ISBN-10: 0471478180.

[69] M. Palacios, Y.F. Houst, P. Bowen, F. Puertas, Adsorption of superplasticizer admixtures on alkali-activated slag pastes, Cement and Concrete Research 39 (8) (2009) 670–677.

[70] Sant, G., Scrivener, K. L., and Weiss, W. J., 'Unpublished Results', Experiments performed at Purdue University and the Ecole Polytechnique Federale De Lausanne, January-December, (2005-2009).

[71] F. Merlin, H. Guitouni, H. Mouhoubi, S. Mariot, F. Vallee, H. Van Damme, Adsorption and heterocoagulation of nonionic surfactants and latex particles on cement hydrates, Journal of Colloid and Interface Science 281 (2005) 1–10.

[72] D. Damidot, F.P. Glasser, Thermodynamic investigation of the $CaO-Al_2O_3-CaSO_4-H_2O$ system at 50 °C and 85 °C, Cement and Concrete Research 22 (76) (1992) 1179–1191.

[73] D. Damidot, F.P. Glasser, Thermodynamic investigation of the $CaO-Al_2O_3-CaSO_4-H_2O$ system at 25 °C, Cement and Concrete Research 23 (1) (1993) 221–238.

[74] J.J. Thomas, D. Rothstein, H.M. Jennings, B.J. Christensen, Effect of hydration temperature on the solubility behavior of Ca-, S-, Al- and Si- bearing solid phases in Portland cement pastes, Cement and Concrete Research 33 (12) (2003) 2037–2047.

[75] B. Lothenbach, T. Matschei, G. Moschner, F.P. Glasser, Thermodynamic modeling of the effect of temperature on the hydration and porosity of Portland cement, Cement and Concrete Research 38 (1) (2008) 1–18.
[76] S. Diamond, Long term status of calcium hydroxide saturation of pore solutions of hardened cements, Cement and Concrete Research 5 (1975) 607–616.
[77] G.W. Scherer, Crystallization in pores, Cement and Concrete Research 29 (1999) 1347–1358.
[78] M. Steiger, Crystal growth in porous materials I: the crystallization pressure of large crystals, Journal of Crystal Growth 282 (2005) 455–469.
[79] R.J. Flatt, G.W. Scherer, Thermodynamics of crystallization stresses in DEF, Cement and Concrete Research 38 (2008) 325–336.
[80] R.J. Flatt, Salt damage in porous materials: how high supersaturations are generated, Journal of Crystal Growth 242 (2002) 435–454.
[81] P. Mounanga, V. Baroghel-Bouny, A. Loukili, A. Khelidj, Autogenous deformations of cement pastes: Part 1. temperature effects at early age and micro–macro correlations, Cement and Concrete Research 36 (1) (2006) 110–122.
[82] V. Baroghel-Bouny, P. Mounanga, A. Khelidj, A. Loukili, N. Rafai, Autogenous deformations of cement pastes: Part 2. W/C Effects, micro-macro correlations and threshold values, Cement and Concrete Research 36 (1) (2006) 123–136.
[83] O. Coussy, Deformation and stress from in-pore drying-induced crystallization of salt, Journal of the Mechanics and Physics of Solids 54 (2006) 1517–1547.
[84] Z. Sun, G.W. Scherer, Effect of air voids on salt scaling and internal freezing, Cement and Concrete Research 40 (2010) 260–270.
[85] W.A. Gutteridge, J.A. Dalziel, Filler cement: the effect of the secondary component on the hydration of Portland cement: Part 1: A fine non-hydraulic filler, Cement and Concrete Research 20 (5) (1990) 778–782.
[86] G.W. Scherer, Stress from crystallization of salt, Cement and Concrete Research 34 (2004) 1613–1624.
[87] N.B. Singh, B. Middendorf, Calcium sulfate hemihydrate hydration leading to gypsum crystallization, Progress in Crystal Growth and Characterization of Materials 53 (1) (2007) 57–77.
[88] K. Riding, D. Silva, K.L. Scrivener, 'Early Age Strength Enhancement of Blended Cement Systems by $CaCl_2$ and Diethanol-isopropanolamine', Cement and Concrete Research 40 (6) (2010) 935–946.
[89] P. Lura, O.M. Jensen, K. van Breugel, Autogenous shrinkage in high-performance cement paste: an evaluation of basic mechanisms, Cement and Concrete Research 33 (2) (2003) 223–232.
[90] O.M. Jensen, P.F. Hansen, Water-entrained cement based materials I: Principles and theoretical background, Cement and Concrete Research 31 (4) (2001) 647–654.
[91] P. Lura, J. Couch, O.M. Jensen, W.J. Weiss, Early-age acoustic emission measurements in hydrating cement paste: evidence for cavitation during solidification due to self-desiccation, Cement and Concrete Research 39 (10) (2009) 861–867.
[92] Dehadrai, M., 'Health Monitoring of Civil Engineering Materials', MSCE Thesis, Purdue University, West Lafayette, IN, USA, (2008).
[93] J.K. Mackenzie, The elastic constants of a solid containing spherical holes, Proceedings of the Physical Society – Section B 63 (1950) 2–11.
[94] D. Bentz, E.J. Garboczi, D.A. Quenard, Modeling drying shrinkage in reconstructed porous materials: application to porous Vycor glass, Modeling and Simulation in Materials Science and Engineering 6 (1998) 211–236.
[95] L.F. Nielsen, A research note on sorption, pore size distribution and shrinkage of porous materials, Building Materials Laboratory, The Technical University of Denmark, Lyngby, Denmark, 1991., Technical Report 245/91.
[96] Z.C. Grasley, G.W. Scherer, D.A. Lange, J.J. Valenza, Dynamic pressurization method for measuring permeability and modulus: II. Cementitious materials, Materials and Structures 40 (2007) 711–721.
[97] G. Sant, M. Dehadrai, D. Bentz, P. Lura, C.F. Ferraris, J. Bullard, W.J. Weiss, Detecting the fluid-to-solid transition in cement pastes, Concrete International (June 2009) 43–48.
[98] I. Vlahinic, H.M. Jennings, J.J. Thomas, A constitutive model for drying of a partially saturated porous material, Mechanics of Materials 41 (3) (2009) 319–328.
[99] M. Steiger, Crystal growth in porous materials II: Influence of crystal size on the crystallization pressure, Journal of Crystal Growth 282 (2005) 470–481.
[100] M. Balonis, F.P. Glasser, The density of cement phases, Cement and Concrete Research 39 (9) (2009) 733–739.
[101] J.J. Thomas, H.M. Jennings, Changes in the size of pores during shrinkage (or expansion) of cement paste and concrete, Cement and Concrete Research 33 (2003) 1897–1900.